Journal of The Electrochemical Society, **147** (6) 2303-2311 (2000)
S0013-4651(00)02-051-6 CCC: $7.00 © The Electrochemical Society, Inc.

Numerical Modeling of Gas-Phase Nucleation and Particle Growth during Chemical Vapor Deposition of Silicon

S. L. Girshick, M. T. Swihart,*,[a] S.-M. Suh, M. R. Mahajan, and S. Nijhawan

Department of Mechanical Engineering, University of Minnesota, Minneapolis, Minnesota 55455, USA

A numerical model was developed to predict gas-phase nucleation of particles during silane pyrolysis. The model includes a detailed clustering mechanism for the formation of hydrogenated silicon clusters containing up to ten silicon atoms. This mechanism was coupled to an aerosol dynamics moment model to predict particle growth, coagulation, and transport. Both zero-dimensional transient simulations, at 1-2 atm pressure, and one-dimensional steady-state stagnation-point flow simulations, at 1-2 Torr pressure, were conducted. The effects of carrier gas, temperature, pressure, silane concentration, and flow rate were examined. The results predict that hydrogen as carrier gas, compared to helium, suppresses nucleation, and that particle formation for the case of hydrogen carrier gas increases strongly with increasing initial silane-to-hydrogen ratio. For the conditions examined, predicted particle nucleation rates increase dramatically with increasing temperature. The effect of total pressure depends on the pressure regime: at 1-2 atm pressure particle formation is predicted to be insensitive to pressure, whereas at 1-2 Torr particle formation is predicted to increase strongly with increasing pressure. The predicted effects on particle formation of temperature, pressure, carrier gas, and silane concentration are all qualitatively consistent with published experimental results. In the stagnation-point flow simulations the flow rate is found to affect particle dynamics because of the opposed effects of convective transport toward the heated water and thermophoretic transport away from the wafer.

Manuscript received February 16, 2000.

The growth of silicon films via chemical vapor deposition (CVD) is of considerable importance in the microelectronics and photovoltaics industries. This process often involves the thermal decomposition of silane, which is achieved by heating the wafer or rod to be coated to a suitable temperature. A wide range of geometries and conditions are employed. For example, low-pressure chemical vapor deposition (LPCVD), at pressures around 1 Torr (133 Pa), is used with a stagnation-point flow geometry to deposit thin films of silicon in the fabrication of integrated circuits, while cylindrical polysilicon rods are grown on a heated filament using atmospheric-pressure CVD (APCVD).

A frequent by-product of silicon CVD is the formation of powder from gas-phase particle nucleation. In most cases gas-phase nucleation is viewed as an undesirable phenomenon which limits film growth rates because it represents a source of contamination. In other cases it is a deliberate means to the production of nanostructured materials for their desirable properties.

A few studies have previously been reported in which particle formation from silicon hydrides during silane pyrolysis was modeled. Yuuki *et al*.[1] presented a simple mechanism that included species containing up to five silicon atoms and formation of particles directly from Si_5H_{12}. Giunta *et al*.[2] proposed a mechanism that included linear silanes (saturated Si_nH_{2n+2}), silylenes (divalent Si_nH_{2n}), and silenes (Si_nH_{2n} with a formal double bond) containing up to ten silicon atoms. Frenklach *et al*.[3] developed a similar but somewhat larger mechanism. In both of these latter studies the rate coefficients for reactions involving silanes and silylenes containing more than two silicon atoms were assumed to be identical to those for the analogous reaction of disilane. Cyclic species were not considered. Reactions for which the sum of the silicon atoms in the reactants exceeded ten were assumed to from "particles." In the study by Frenklach *et al*.[3] a particle growth model was included, in which sticking coefficients for silanes, SiH_2, and H_3SiSiH were based on values in the literature for silicon film growth. Sticking coefficients for several other species were estimated by matching the model results to the authors' experimental results for particles produced in a shock tube.

Recently Swihart and Girshick presented a detailed mechanism for silicon hydride clustering during silane pyrolysis.[4] Relative to the studies discussed above this mechanism utilizes far more detailed information regarding the thermodynamic properties and reactivities of silicon hydride clusters. In addition, this mechanism includes cyclic and polycyclic clusters, which had been neglected in previous work. These species were predicted to be particularly stable, and thus to play a key role in the nucleation process.

In the work presented here we have coupled this clustering mechanism to a model which solves the aerosol general dynamics equation to predict the evolution of the moments of the particle size distribution function, accounting for particle growth, coagulation, and transport. We present results both of zero-dimensional (time-dependent) simulations under conditions typical of APCVD, and of one-dimensional steady-state simulations under conditions typical of LPCVD in a stagnation-point flow geometry.

Description of Model

Chemical clustering model.—A detailed description of our reaction mechanism has been presented elsewhere.[4] Briefly, the mechanism considers reversible reactions among silicon hydrides containing up to ten silicon atoms. The silicon hydrides considered are shown in Fig. 1. They include acyclic, cyclic and polycyclic silanes, silylenes, and silenes. For each stoichiometry, the most stable isomer of each type (silane, silene, and silylene) is considered and its thermochemical properties are taken to represent all isomers of that stoichiometry and type. Other isomers are not explicitly considered.

Table I summarizes the reactions we considered and their associated rate parameters. For reactions among species containing one or two silicon atoms (Si, SiH_2, SiH_4, H_2SiSiH_2, H_3SiSiH, Si_2H_6) we use the reactions and rate parameters recommended by Ho *et al*.[5] These are Reactions 1-11 in Table I. (In the notation of Fig. 1, H_2SiSiH_2 and H_3SiSiH are, respectively, denoted Si_2H_4A and Si_2H_4B). This mechanism explicitly treats the pressure dependence of the unimolecular decomposition and recombination reactions with the pressure dependence parameterized in the form recommended by Troe.[6] It is the most complete and thoroughly validated of the detailed mechanisms for silane decomposition that have been presented in the literature.

Reactions in the mechanism involving larger silicon hydrides can be grouped into five classes: (*i*) hydrogen elimination from silanes (and its reverse, silylene insertion into hydrogen); (*ii*) silylene elimination from silanes (and its reverse, silylene insertion into a silane to form a larger silane); (*iii*) silylene elimination from silenes (and its reverse, silylene insertion into a silene to form a larger silene);

* Electrochemical Society Active Member.
[a] Present address: Department of Chemical Engineering, University at Buffalo (SUNY), Buffalo, NY 14260-4200, USA.

S0013-4651(00)02-051-6 CCC: $7.00

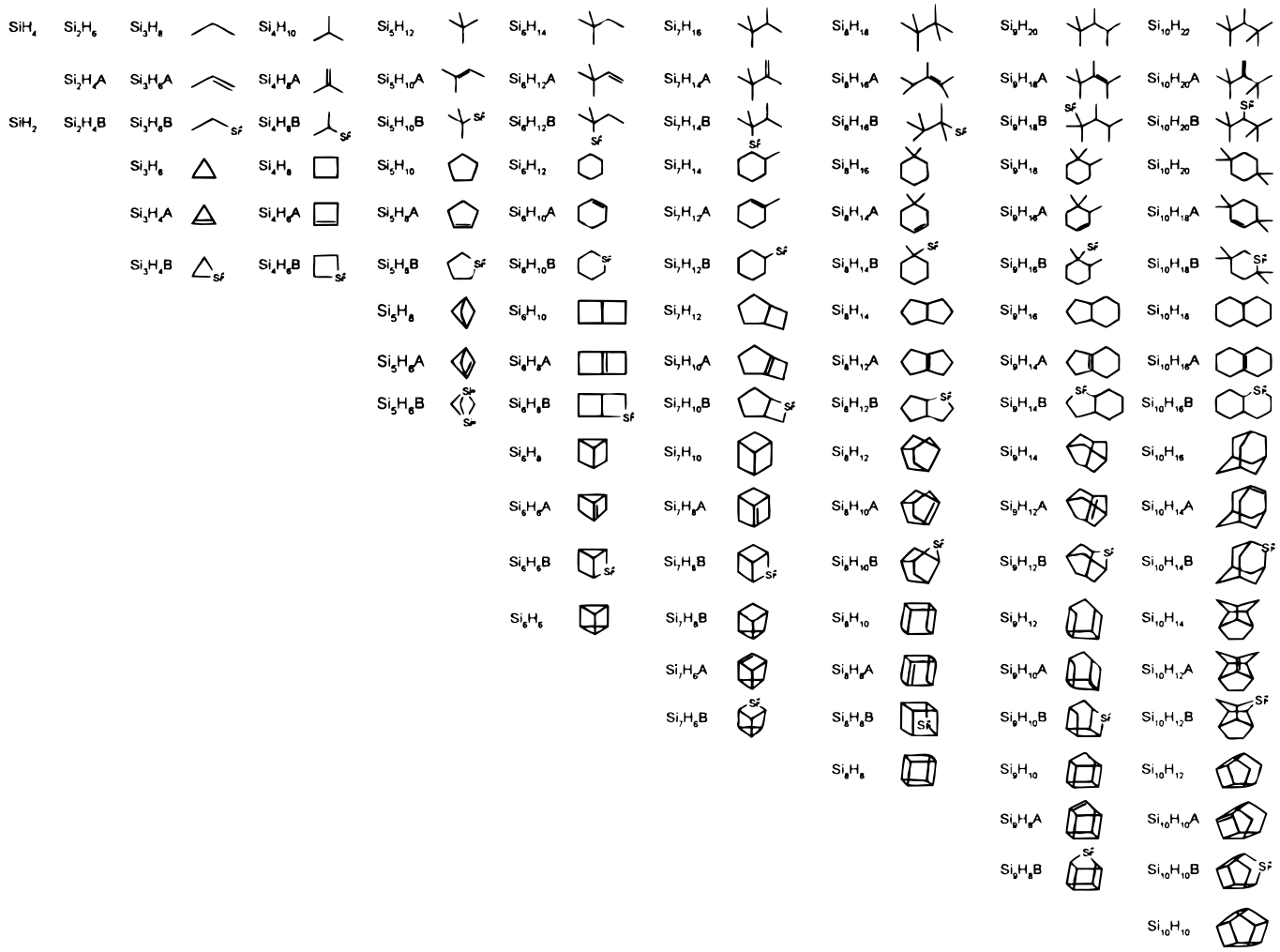

Figure 1. Silicon hydrides in mechanism. Compounds without a suffix are fully saturated silanes. Silenes are denoted with an "A" suffix, silylenes with a "B" suffix.

(*iv*) ring opening (and its reverse, ring formation by intramolecular insertion); and (*v*) silylene-to-silene isomerization. These five reaction classes are shown as Reactions 12 through 16 in Table I. Each reaction type is applied to all of the appropriate species from Fig. 1, yielding the number of reactions of each type indicated in Table I.

The first four of these reaction types all involve, in their reverse direction, silylene insertions into Si–H bonds or H_2. A number of studies, reviewed in more detail in Swihart and Girshick,[4] indicate that these insertions are barrierless. Insertion reactions of SiH_2 with H_2, SiH_4, Si_2H_6, and Si_3H_8 have been studied experimentally, and all have small negative activation energies and rate parameters close to the collision rate (in the high pressure limit) indicating that they are barrierless processes.[7] The forward reactions (*i.e.*, silylene eliminations) are thus expected to have activation energies approximately equal to the enthalpy of reaction. This has been confirmed by experimental[8-12] and theoretical[12-16] studies of the thermal decomposition of SiH_4, Si_2H_6, Si_3H_8, and Si_4H_{10}. We have taken the activation energies for these reactions to be independent of temperature and equal to the corresponding heats of reaction at 1000 K. For all reactions of this type we assumed a pre-exponential factor of 2×10^{15} s^{-1}, based on the known values for decomposition of the small compounds that have been studied experimentally. For Reactions 1 through 5 in Table I, the high pressure pre-exponential factors at 1000 K are 1.6×10^{15} s^{-1}, 2.3×10^{15} s^{-1}, 2.3×10^{15} s^{-1}, 7.0×10^{15} s^{-1}, and 3.4×10^{15} s^{-1}, respectively. All these reactions proceed through similar three-centered transition states, and the value of the pre-exponential factor is essentially determined by the difference in structure between the reactant and the transition state.[17] We expect that the actual pre-exponential factor for individual reactions would range from about a factor of five larger (for particularly loose transition states) to a factor of five smaller (for particularly tight transition states) than our estimate of 2×10^{15}. However, variations outside that range would require that the reaction go through a transition state structure that is substantially different from that of the smaller molecules, and there is no reason to expect such a change in reactivity. For all silylene-to-silene isomerizations we have assumed a forward rate coefficient with a pre-exponential factor of 10^{13} s^{-1} and an activation energy of 7.5 kcal/mol (31.4 kJ/mol), based on an *ab initio* electronic structure calculation for Si_2H_4B isomerization to Si_2H_4A. [18] Little is known experimentally about these reactions, however, at temperatures high enough for silane pyrolysis to occur these isomerization reactions are much faster than any other reactions in our mechanism. Because of this, they are near equilibrium in all of our simulations, and our results are insensitive to the selection of rate parameters for them. Our results are somewhat sensitive to the thermochemical properties of these species, since these determine the relative concentrations of the isomers at equilibrium.

Rate constants for all reverse reactions were calculated as the ratio of the forward rate constant to the equilibrium constant. The temperature-dependent heats of reaction and entropies of reaction, obtained from the thermochemical properties calculated as discussed below, were used in calculating the equilibrium constants.

We estimated the standard enthalpies of formation, standard entropies, and heat capacities of the compounds shown in Fig. 1 by

S0013-4651(00)02-051-6 CCC: $7.00

Table I. Gas phase and clustering reaction mechanism. Forward rate constants are expressed in the form $k_f = AT^{\beta} \exp(-E_a/RT)$.

	Reaction	A (cm^3 mol, s)	β	E_a (cal/mol)	References/notes
	Base mechanism (11 reactions)				
1.	SiH_4 (+M) = SiH_2 + H_2 (+M)				
	High-pressure limit:	3.12E + 09	1.7	54710	a, b
	Low-pressure limit:	521E + 29	−3.54	57550	
	Troe parameters:				
	a = −0.4984, T^{***} = 888.3, T^{*} = 209.4, T^{**} = 2760.0				
	Enhanced third-body efficiencies:				
	SiH_4 = 4, Si_2H_6 = 4				
2.	Si_2H_6 (+M) = SiH_4 + SiH_2 (+M)				
	High-pressure limit:	1.81E + 10	1.7	50203	a, b
	Low-pressure limit:	5.09E + 53	−10.37	56034	
	Troe parameters:				
	a = 4.375E-5, T^{***} = 438.5, T^{*} = 2726.0, T^{**} = 438.2				
	Enhanced third-body efficiencies:				
	SiH_4 = 4, Si_2H_6 = 4				
3.	Si_2H_6 (+M) = H_2 + Si_2H_4B (+M)				
	High-pressure limit:	9.09E + 09	1.8	54197	a, b, c
	Low-pressure limit:	1.94E + 44	−7.77	59023	
	Troe parameters:				
	a = −0.1224, T^{***} = 793.3, T^{*} = 2400.0, T^{**} = 11.39				
	Enhanced third-body efficiencies:				
	SiH_4 = 4, Si_2H_6 = 4				
4.	Si_3H_8 (+M) = SiH_2 + Si_2H_6 (+M)				
	High-pressure limit:	6.97E + 12	1	52677	a, b
	Low-pressure limit:	1.73E + 69	−15.07	60491	
	Troe parameters:				
	a = −3.47E-5, T^{***} = 442.0, T^{*} = 2414.0, T^{**} = 128.3				
	Enhanced third-body efficiences:				
	SiH_4 = 4, Si_2H_6 = 4				
5.	Si_3H_8 (+M) = SiH_4 + Si_2H_4B (+M)				
	High-pressure limit:	3.73E + 12	1	50850	a, b, c
	Low-pressure limit:	4.36E + 76	−17.26	59303	
	Troe parameters:				
	a = 0.4157, T^{***} = 365.3, T^{*} = 3102.0, T^{**} = 9.72				
	Enhanced third-body efficiences:				
	SiH_4 = 4, Si_2H_6 = 4				
6.	Si_2H_4B (+M) = Si_2H_4A (+M)				
	High-pressure limit:	2.54E + 13	−0.2	5381	a, b, c
	Low-pressure limit:	1.10E + 33	−5.76	9152	
	Troe parameters:				
	a = −0.4202, T^{***} = 214.5, T^{*} = 103.0, T^{**} = 136.3				
	Enhanced third-body efficiences:				
	SiH_4 = 4, Si_2H_6 = 4				
7.	Si_2H_4B + H_2 = SiH_2 + SiH_4	9.41E + 13	0	4092.3	a, b, c
	Reverse	9.43E + 10	1.1	5790.3	
8.	Si_2H_4B + SiH_4 = Si_2H_6 + SiH_2	1.73e + 14	0.4	8898.7	a, b, c
	Reverse	2.65E + 15	0.1	8473.4	
9.	Si_2H_4B (+M) = Si + SiH_4 (+M)				
	High-pressure limit:	1.42E + 13	0.54	57548	a, b, c
	Low-pressure limit:	2.35E + 42	−7.42	60957	
	Troe parameters:				
	a = 0.5336, T^{***} = 629.2, T^{*} = 2190.0, T^{**} = 626.5				
	Enhanced third-body efficiences:				
	SiH_4 = 4, Si_2H_6 = 4				
10.	Si + Si_2H_6 = SiH_2 + Si_2H_4B	1.30E + 15	0	12600	a, b, c
11.	SiH_2 + M = Si + H_2 + M	9.10E + 20	−1.76	38241	a, b
	Hydrogen elimination (33 reactions)				
12.	Si_nH_{2m} = $S_nH_{2(m-1)}B$ + H_2	2.00E + 15	0	$\Delta H_{rxn,1000K}$	c, d, e
	Silylene elimination from saturated silicon hydrides (149 reactions)				
13.	Si_nH_{2m} = $S_nH_{2k}B$ + $Si_{(n-j)}H_{2(m-k)}$	2.00E + 15	0	$\Delta H_{rxn,1000K}$	c, d, e
	Silylene elimination from silene (163 reactions)				
14.	Si_nH_{2m} = $S_jH_{2k}B$ + $Si_{(n-j)}H_{2(m-k)}A$	2.00E + 15	0	$\Delta H_{rxn,1000K}$	c, d, e

Table I (*continued on next page*)

S0013-4651(00)02-051-6 CCC: $7.00

Table I. *(continued)*

Reaction	A (cm^3 mol, s)	β	E_a (cal/mol)	References/notes
Silylene to silene isomerization (33 reactions)				
15. $Si_nH_{2m}B = S_nH_{2m}A$	1.00E + 13	0	7500	c, e
Ring opening/formation (28 reactions)				
16. $Si_nH_{2m} = S_nH_{2m}B$ ($n \geq 3$)	2.00E + 15	0	$\Delta H_{rxn,1000K}$	c, d, e
Irreversible particle formation				
17. $Si_nH_{2m} + S_jH_{2k}B \rightarrow$ particle ($n + j \geq 11$)	1.60E + 13	0.5	0	c, e
18. $Si_nH_{2m}A + S_jH_{2k}B \rightarrow$ particle ($n + j \geq 11$)	1.60E + 13	0.5	0	c, e

[a] P. Ho, M. E. Coltrin and W. G. Breiland, *J. Phys. Chem.*, **98**, 10138 (1994).
[b] Falloff reactions in the Troe form [R. G. gilbert, K. Luther, and J. Troe, *Ber. Bunsenges. Phys. Chem.*, **87**, 169 (1983).
[c] Molecules with an A suffix are silenes. Molecules with a B suffix are silylenes.
[d] $\Delta H_{rxn,1000K}$ is the heat of reaction at 1000 K.
[e] *n*, *m*, *j*, and *k* are integers.

applying a group additivity scheme, based on the *ab initio* molecular orbital calculations of Katzer *et al*.[9] of 143 silicon hydrides containing up to five silicon atoms. The heats of formation predicted from the calculations of Katzer *et al*. agree with experimental values to within the uncertainty of the experimental values for all of the species for which experimental heats of formation are known (SiH_4, SiH_3, SiH_2, SiH, Si_2H_6, Si_2H_5, Si_2H_4A, Si_2H_4B, and Si_3H_8), except for Si_2H_4A, for which the prediction is 0.5 kcal/mol above the upper error limit of the experimental value. In the group additivity scheme, twenty-six groups were defined, and values for the enthalpy of formation at standard conditions, the standard entropy and the heat capacity at 300, 400, 500, 600, 800, 1000, and 1500 K for each of these groups were determined by a linear least-squares fit to the Katzer *et al*. data. For a given molecule, each of these properties is the sum of contributions of the groups that comprise it. Detailed descriptions of this kind of group additivity scheme and its application to hydrocarbons are given by Benson[17] and by Ritter and Bozzelli.[20] Given the enthalpy of formation, standard entropy, and temperature-dependent heat capacity for an ideal gas, one can obtain the enthalpy, entropy, and all other thermodynamic quantities at any desired temperature and pressure (within the temperature range for which the heat capacity is known). The group additivity approach was checked by conducting *ab initio* electronic structure calculations of eight compounds containing 6-10 silicon atoms at a moderately high level of theory that, in other benchmark tests, predicts heats of formation to within an average absolute deviation of 1.7 kcal/mol.[21] The thermodynamic property data base thus developed was used to estimate the enthalpies of reaction, which were used in the forward rate coefficients as described above, and the Gibbs free energies of reaction, which were used to determine all reverse rate coefficients via the equilibrium constant. Both the group additivity parameters and the resulting estimates of species properties are tabulated in Swihart and Girshick.[4] Thermodynamic properties for all species in the mechanism were expressed in terms of polynomial coefficients[b] in the standard NASA format used by the CHEMKIN family of codes.[22]

Swihart and Girshick[4] also considered, as a parallel reaction path, self-nucleation of silicon particles via a pure silicon clustering pathway, that is, through reactions of the form $Si_n + Si \leftrightarrow Si_{n+1}$. However, for all of the conditions they considered) which correspond to the conditions considered here), it was found that the pure silicon clustering pathway made a negligible contribution to particle formation. Therefore, the simulations presented here neglect this reaction path. However, we expect this route to be more important under higher temperature conditions, for example, as might occur in thermal plasmas or in laser-induced pyrolysis, where silicon particles may nucleate at temperatures exceeding 2000 K. [23] Such conditions favor high concentrations of silicon vapor and hydrogen elimination from silicon hydrides, both of which would increase the importance of pure silicon clustering.

The version of the mechanism utilized here considers approximately 100 species, containing up to ten silicon atoms, undergoing approximately 400 reversible reactions. (Slightly different versions were run for the two different pressure regimes for which the numerical simulations presented below were conducted.) In addition we include irreversible reactions, assumed to occur at the gas kinetic rate, that produce compounds having more than ten silicon atoms. In Swihart and Girshick[4] all such possible reactions were included, for a total of 2614 reactions, which thus produced compounds having 11-20 silicon atoms. In the present work we include only those reactions that produce compounds having 11-13 silicon atoms, thereby reducing the total number of reactions to approximately 1000. This produced a negligible change in the results while greatly decreasing the computational effort required to implement the models.

It should be emphasized that the truncation of our reversible reaction mechanism at size ten is arbitrary. We expect that relatively stable silicon hydrides exist at larger sizes, and that these compounds would, under many conditions, represent bottlenecks to nucleation. For example, we found that the particle nucleation rates predicted by the mechanism truncated at size ten were typically about three orders of magnitude lower than those predicted when we truncated at size five. Thus we expect, within the assumptions and inherent uncertainties of our mechanism, that the nucleation rate is in general overpredicted. Nevertheless, it is reasonable to expect that those conditions that increase or decrease the production rate of compounds having more than ten silicon atoms would have a corresponding effect on the production rate of compounds having, say, more than 20 silicon atoms. Thus the predicted nucleation rates are expected to show qualitative trends, and to represent an approximate upper bound on the true nucleation rate.

Aerosol dynamics model.—The gas-phase kinetics model described above was self-consistently coupled to an aerosol dynamics model. That is, the rate of production of compounds containing more than ten silicon atoms was taken as a particle source term in the aerosol dynamics model, and particle growth by surface chemical reactions was calculated using species concentrations determined by the gas-phase model. Conversely, the gas-phase model accounted for species depletion due to particle nucleation and growth.

Aerosol dynamics were modeled using a moment-type formulation, which casts the aerosol general dynamics equation into separate equations for the first few moments of the particle size distribution

[b] Available upon request from SLG: slg@tc.umn.edu

S0013-4651(00)02-051-6 CCC: $7.00

function.[24-30] The moment approach offers a computationally efficient means of simulating aerosol dynamics, which is particularly desirable given the complexity of our chemical clustering mechanism.

Let M_k represent the kth moment of the size distribution, defined by

$$M_k = \int_0^\infty v_p^k n(v_p) dv_p \quad [1]$$

where v_p is particle volume and $n(v_p)$ is the particle size distribution function. Thus, the zeroth moment represents the total particle concentration, the first moment equals the particle volume fraction (volume of particles per unit volume of gas), and the ratio M_1/M_0 equals the number-mean particle volume.

In terms of the effects pertinent to the conditions considered in this work, the aerosol general dynamic equation in moment formulation can be written as

$$\frac{\partial M_k}{\partial t} + \rho_g \mathbf{u}\cdot\nabla\left(\frac{M_k}{\rho_g}\right) = \left(\dot{M}_k\right)_{\text{nucleation}} + \left(\dot{M}_k\right)_{\text{surface reactions}} + \left(\dot{M}_k\right)_{\text{coagulation}} + \left(\dot{M}_k\right)_{\text{diffusion}} + \left(\dot{M}_k\right)_{\text{thermophoresis}} \quad [2]$$

where ρ_g is gas density, $\mathbf{u}$ is bulk fluid velocity, and the terms on the right side represent rates of change of the kth moment due, respectively, to nucleation, growth by surface reactions, coagulation, and transport by Brownian diffusion and thermophoresis.

We have adopted a similar moment formulation as described by Pratsinis and co-workers.[28-30] A closed set of equations for the moments of the size distribution is obtained by assuming that the distribution follows a lognormal form. In this formulation it suffices to solve Eq. 2 for just the first three moments of the size distribution, M_0, M_1, and M_2. From this one obtains the main quantities of interest, including total particle concentration, mean particle size, and geometric standard deviation of the size distribution.

A new aspect of the present work is that whereas previous studies using moment-type models have assumed that particle growth occurred by condensation of supersaturated vapor, we treated particle growth as a chemical vapor deposition process. As noted in the previous section, self-clustering of silicon vapor was found to make only a negligible contribution to particle formation compared to chemical clustering of silicon hydrides. We similarly find that silicon vapor is predicted to exist in too small concentrations to make a significant contribution to particle growth. On the other hand, it is reasonable to suppose that a particle in our system can grow by the same kinetic mechanisms as a chemical vapor deposited film. Thus, for the term representing particle growth by surface reactions we use the silicon film growth mechanism presented in Ho *et al*.,[5] which is also the mechanism we utilize for film growth on the substrate in the stagnation-point flow simulations presented below. That mechanism was developed specifically so that, together with their gas-phase reaction mechanism, a good fit was obtained to experimental data on silicon deposition rates in a CVD reactor. Use of this model for particle growth is probably reasonable (within the model's uncertainties) for particles once they are larger than a few nanometers in diameter, but is obviously an imperfect approximation when applied to particles as small as our "nuclei," which contain only 11-13 silicon atoms. Nevertheless, it seems preferable to employ a surface growth model at these small sizes rather than to neglect surface growth (and thus, to include only coagulation), as the conditions under which high rates of nucleation occur, namely, the existence of high concentrations of reactive species, are essentially the same as those under which one would expect significant growth by surface reactions.

In the simulations presented below for which the pressure is either 1 or 2 Torr the particles are much smaller than the mean free path for collisions in the gas, and the standard free molecule regime expressions are used for coagulation, diffusion, and thermophoresis.[31] For the simulations at 1 or 2 atm pressure, particles in some cases lie in the regime of transitional Knudsen number. These latter simulations, being zero-dimensional, did not involve particle transport, but did include coagulation, for which we used an interpolation formula for the transition regime, in which the coagulation coefficient is based on the harmonic average of the coagulation coefficients for the free molecule and continuum regimes.[29]

Numerical Simulations

We conducted two types of simulations. Zero-dimensional, time-dependent simulations at fixed temperature and pressure were conducted, under conditions typical of silane pyrolysis around atmospheric pressure, starting at time zero with a dilute concentration of silane in hydrogen or helium. In addition we conducted stagnation-point flow simulations, under conditions typical of LPCVD in a GEC reference cell. In these simulations a cold gas consisting of pure silane flows toward a heated substrate. Both the showerhead gas inlet and the substrate have a 10.16 cm diam, the distance from the inlet to the substrate is 6.8 cm, and the gas temperature at the inlet is in all cases set to 423 K.

Both types of simulations utilized the Chemkin family of codes, with the transient simulations using Senkin,[32] while the stagnation-point flow simulations used the Spin code.[33] Computer run times ranged from ~5 min to a Silicon Graphics Origin 200, for the zero-dimensional simulations, to ~15 h on a Silicon Graphics Origin 2000, for the stagnation-point flow simulations, though it should be pointed out that our code could undoubtedly be improved to take better advantage of parallel processing capabilities.

Results

In the zero-dimensional simulations, we examined the effects of temperature, pressure, initial silane concentration, and hydrogen *vs*. helium as carrier gas. Figures 2 and 3 show the predicted evolution of silicon hydride clustering for silane diluted in helium and hydrogen, respectively. In each case the conditions are fixed at a temperature and pressure of 1023 K, 1 atm, and the initial silane mole fraction is 1%. In these figures the concentrations of all species containing a given number of silicon atoms are added together. For example, the curve labeled "8" groups together all 16 species in the mechanism containing eight silicon atoms. In both figures one observes a systematic progression in the rise of species containing increasing numbers of silicon atoms. However, it is observed that clustering is sharply suppressed in hydrogen compared to the case for helium, consistent with experimental observations in a study of atmospheric-pressure silane pyrolysis by Slootman and Parent.[34] The cause of suppression by hydrogen can be clearly understood with reference to the clustering mechanism, which includes many hydrogen elimination reactions, starting with $SiH_4 = SiH_2 + H_2$. An increase in the

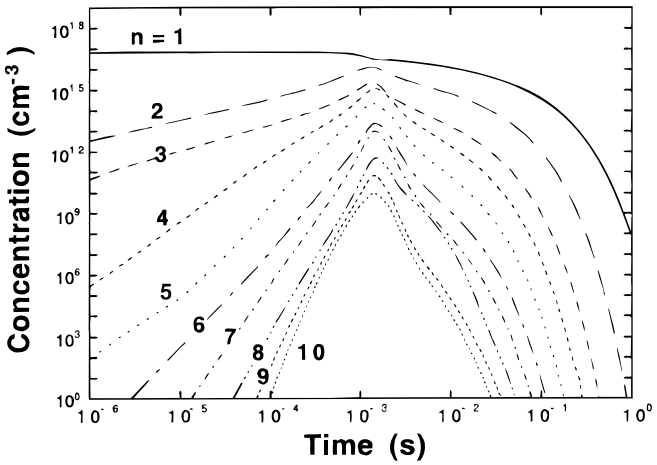

Figure 2. Predicted evolution of concentrations of species containing a given number n of silicon atoms, for 1% silane in helium at 1023 K, 1 atm.

S0013-4651(00)02-051-6 CCC: $7.00

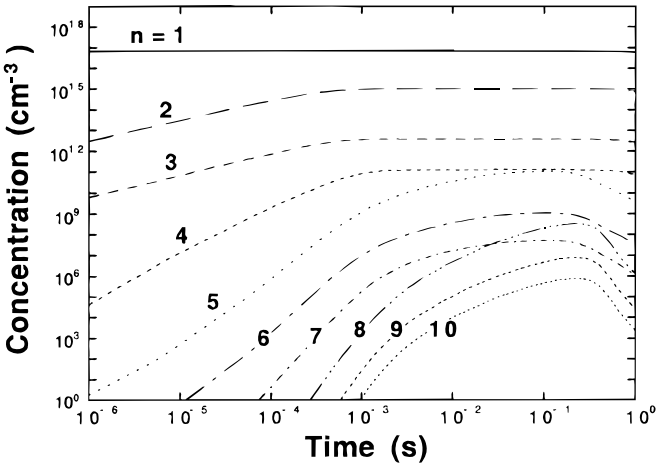

Figure 3. Predicted evolution of concentrations of species containing a given number of silicon atoms, for 1% silane in hydrogen at 1023 K, 1 atm.

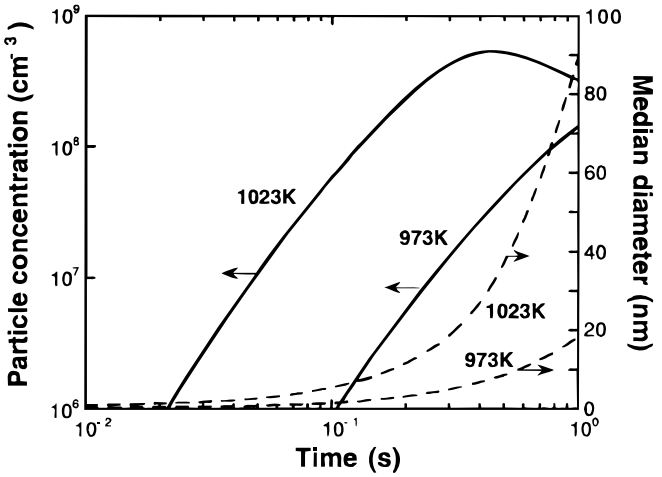

Figure 5. Predicted effect of temperature on particle production for 1% silane in hydrogen at 1 atm.

relative abundance of hydrogen drives these reactions in the reverse direction. Hydrogen is a by-product of the overall clustering process that converts SiH_4 to clusters that have lower hydrogen-to-silicon ratios than SiH_4. Therefore, its use as a carrier gas suppresses the overall clustering process.

In helium the curves all peak shortly past 1 ms and then drop sharply. Two phenomena cause this drop. First, significant silane decomposition occurs at about 1 ms, and other species concentrations tend to scale on silane. Second, at around 1 ms particle nucleation becomes significant, and these particles become a sink for gas-phase species due to surface reactions. In this case, virtually all the silicon in the system is converted to particles in less than 1 s. In hydrogen silane is only slightly decomposed even at 1 s, although some clustering does occur. The declines in the concentrations of the larger species at a few tenths of a second are due to their depletion by particle formation and growth.

Figure 4 shows the predicted particle concentrations and particle sizes (geometric mean diam, hereafter referred to as the "median diam," as for a lognormal distribution it is equivalent to the number-median diam[35]) for the same calculations as for Fig. 2 and 3. In the helium case the particle concentration is predicted to peak at $\sim 10^{12}$ cm^{-3} shortly past 1 ms. The median diam at the time of peak concentration is about 5 nm. The peak in the particle concentration is associated with the quenching of nucleation due to species depletion, as is evident from Fig. 2. Thereafter the particle concentration declines due to coagulation, with a corresponding rise in median diam, predicted to reach about 170 nm after 1 s.

The case of hydrogen carrier gas is again quite different, with significant particle production not predicted until a few milliseconds. The particle concentration in this case peaks around 5×10^8 cm^{-3} at about 0.4 s, and then declines due to coagulation. The predicted median diam after 1 s in the hydrogen case equals 90 nm. The particle volume fraction (total particle volume per unit volume of gas) after 1 s is predicted for the hydrogen case to equal 12% of its value for the helium case.

These simulations predict particle production to be strongly temperature-dependent, again in accord with Slootman and Parent's experimental observations,[34] as shown in Fig. 5, for the case of 1% silane in hydrogen at 1 atm. Around 1000 K an increase of only 50 K is predicted to produce both more particles and much larger particles, about 90 nm at 1 s in the 1023 K case compared to about 18 nm in the 973 K case. The difference in particle size is largely due to the effect of temperature on particle growth rates due to chemical vapor deposition on particle surfaces.

In contrast to the effect of temperature, total pressure is found to have rather little effect, at least in this pressure regime, see below, as seen in Fig. 6, which compares simulations at 1 and 2 atm. In other words, doubling the initial silane partial pressure has little effect, if the ratio of silane to hydrogen is unchanged, whereas increasing the initial silane concentration, at fixed total pressure, has a large effect,

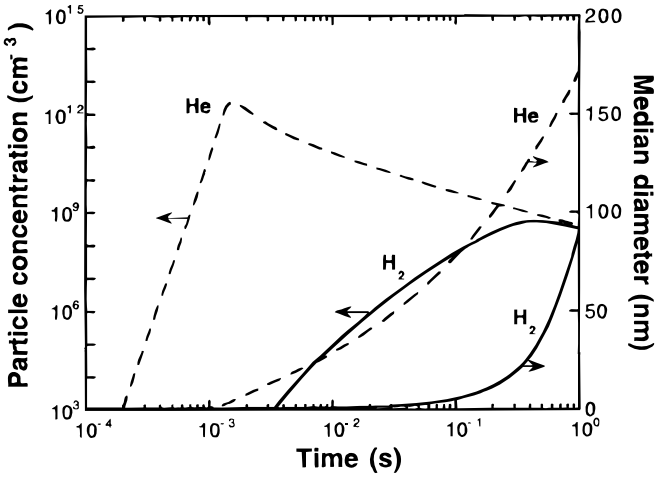

Figure 4. Predicted particle concentration and number-median diam, for 1% silane in either helium or hydrogen at 1023 K, 1 atm.

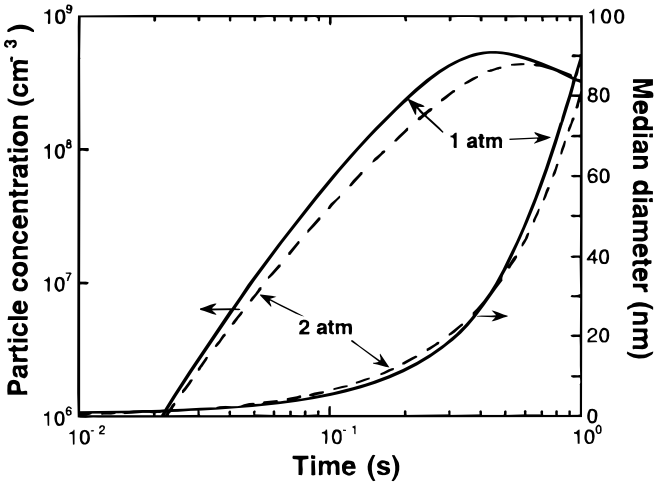

Figure 6. Predicted effect of total pressure on particle production for 1% silane in hydrogen at 1023 K.

S0013-4651(00)02-051-6 CCC: $7.00

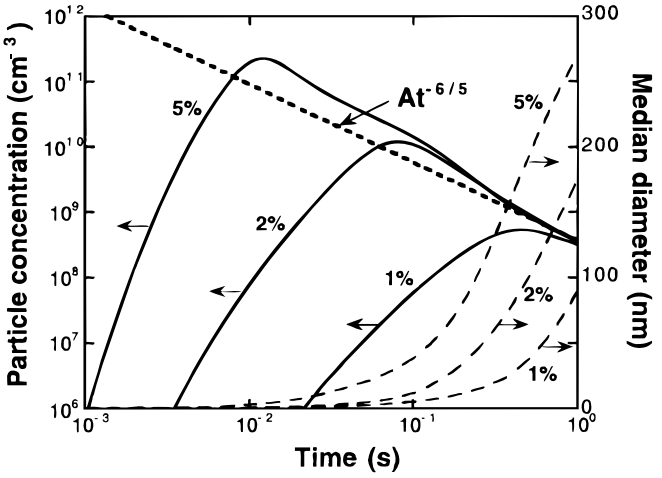

Figure 7. Predicted effect of initial silane mole fraction in hydrogen on particle production at 1023 K, 1 atm.

as seen in Fig. 7. Note that as the initial silane concentration increases the predicted particle volume fraction after 1 s increases much more than linearly: an increase from 1 to 5% silane in hydrogen causes the predicted particle volume fraction to increase by a factor of 30.

All of the particle concentration curves in Fig. 4-7 are observed to peak and then to decline, a consequence of coagulation. For the conditions examined, all of these curves, regardless of particle size, eventually reach remarkably similar values, which at one second are in the 10^8-10^9 cm^{-3} range. The fact that the predicted particle concentrations for this large array of conditions converge is not a coincidence but is rather an expected result of coagulation. Coagulation rates are only weak functions of particle size but are proportional to the square of particle concentration. Thus, in the absence of new particle production or particle losses to walls, coagulation causes the particle concentration curves for these various cases to eventually converge, and thereafter to decline at about the same rate. For this system and for the range of conditions examined in Fig. 4-7, 1 s is predicted to be long enough to observe this effect. Figure 7 also shows that for sufficiently long times all of the particle concentration curves asymptotically approach $N \propto t^{-6/5}$. This behavior is consistent with the predictions of self-preserving size distribution theory[36,37] for an aerosol undergoing Brownian coagulation for particles in the free molecule regime, even though the median particle diameters at $t = 1$ s are large enough to be well into the regime of transitional Knudsen number.

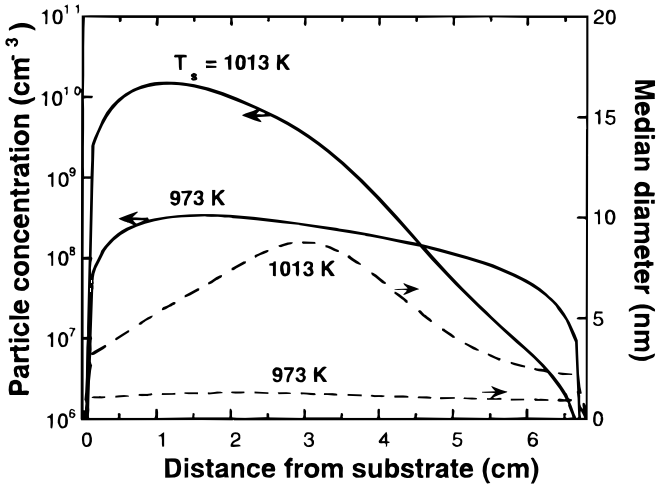

Figure 8. Predicted effect of substrate temperature on spatial profiles of particle concentration and size, for pure silane at 2 Torr, 200 sccm.

Results of the low pressure stagnation-point flow calculations, all for pure silane, are shown in Fig. 8-11. Figure 8 shows the effect of substrate temperature on predicted spatial profiles of particle concentration and median diam, at 2 Torr pressure and a flow rate of 200 sccm. At 973 K the particle production is negligible, although the predicted concentration exceeds 10^8 cm^{-3}, the median diam is everywhere smaller than 1.3 nm. An increase in substrate temperature to 1013 K produces peak concentrations that are higher by two orders of magnitude, and median diam larger than 5 nm.

This result can be compared at least qualitatively to recent measurements[38] made using a particle beam mass spectrometer (PBMS)[39] of particles sampled from the exhaust line of an LPCVD reactor with the same geometry and operating conditions as in these simulations. The PBMS measures a "particle current" which is proportional to the product of the particle concentration and the number-mean particle diam. (The proportionality constant is a complicated function of the instrument. It should be noted that the lower detection limit of the PBMS is about 5 nm in particle diam.) Figure 9a shows the model predictions, for various substrate temperatures, of the product of the particle concentration with the median diam. Figure 9b shows a comparison of these predictions with the PBMS measurements. To make this comparison we integrated the profiles in Fig. 9a, to first order, the aerosol sampled from the exhaust line should correspond to the inte-

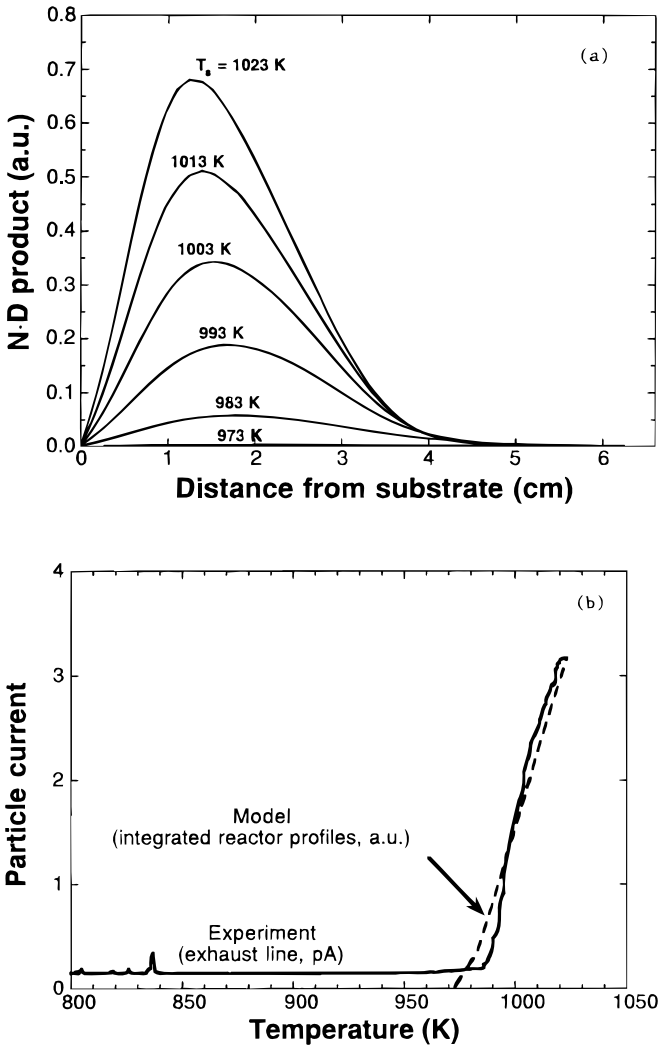

Figure 9. (a) Predicted effect of substrate temperature on spatial profiles of the product of particle concentration and median diam, for pure silane at 2 Torr, 200 sccm, (b) Comparison of the integrated profiles in (a) with experimental measurements of particle current measured by Nijhawan[38] from the exhaust line for the same geometry and conditions.

S0013-4651(00)02-051-6 CCC: $7.00

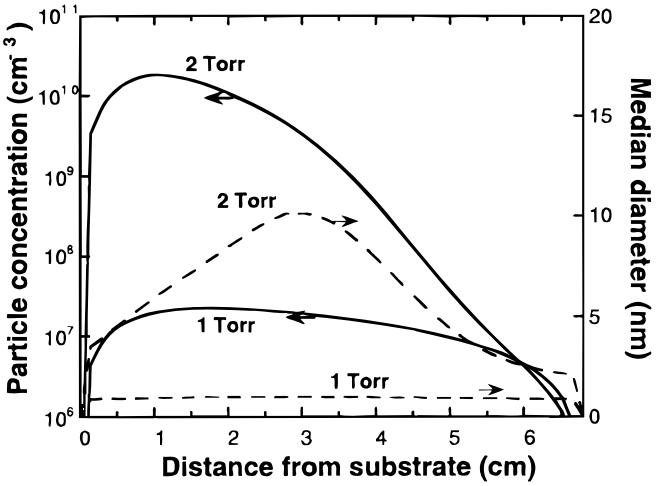

Figure 10. Predicted effect of pressure on spatial profiles of particle concentration and size, for pure silane at 200 sccm and a substrate temperature of 1023 K.

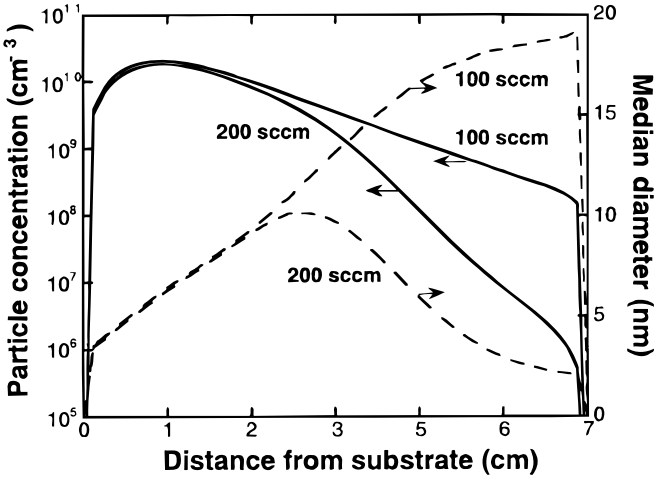

Figure 11. Predicted effect of flow rate on spatial profiles of particle concentration and size, for pure silane at 2 Torr and a substrate temperature of 1023 K.

grated reactor profile, and matched the peak of the predicted particle current (in arbitrary units) to the peak of the measurement (in pA). While this comparison is obviously not quantitative in terms of particle current, it is evident that the experimentally observed trend of particle formation *vs.* temperature is well predicted by the model, as is the quantitative value of the critical temperature for particle formation under these conditions. A more detailed discussion of these experiments and quantitative comparisons with the model predictions will be presented in a subsequent publication.

Figure 10 shows the effect of varying the pressure from 1 to 2 Torr, for a substrate temperature of 1023 K and 200 sccm flow rate. In this case total pressure is seen to have a large effect, contrary to the result for the 1-2 atm pressure range seen in Fig. 6. This result is again in accord with recent PBMS measurements[38] for the same conditions, which found significant particle concentrations at 2 Torr but no signals above noise level at 1 Torr.

The large pressure effect at low pressures is a chemical kinetic rather than a thermodynamic phenomenon. The overall particle formation process produces an increase in the number of moles of gas-phase species as each mole of SiH_4 produces 2 mol of H_2. From the thermodynamic viewpoint lower pressures should therefore favor particle formation. This contrasts with experimental observations and the predictions of this chemical kinetic model, which indicate that particle formation is either favored by increasing pressure (at low pressures)[38] or is insensitive to pressure (at high pressures).[40]

That we find a large pressure effect at low pressure, but little effect at atmospheric pressure, is mainly attributable to the pressure dependence of unimolecular decomposition reactions. Of particular importance is the reaction of silane with silylene, which may follow either of two paths

$$SiH_4 + SiH_2 \rightarrow Si_2H_6^* \rightarrow Si_2H_6 \qquad [3]$$

or

$$SiH_4 + SiH_2 \rightarrow Si_2H_6^* \rightarrow Si_2H_4B + H_2 \qquad [4]$$

Because third-body stabilization of the activated complex is required for the reaction to proceed via Eq. 3, the branching ratio for this reaction pair is pressure-dependent. Based on the rate parameters for these reactions in Table I, together with the reaction equilibrium constants (in Table I these reactions are presented in the reverse direction), one can calculate this branching ratio for various conditions. At 1 atm and 1000 K, 85.4% of the reaction pair proceeds via Eq. 3. At 2 atm there is only a slight increase to 86.4%. In contrast, at 1 Torr and 1000 K only 9.6% of the reaction pair proceeds via Eq. 3, while at 2 Torr this figure almost doubles to 17.2%. (The rate constant for Eq. 3 almost perfectly doubles, as one would expect in the pressure falloff regime.) Thus, at low pressure the reaction given by Eq. 4 constitutes a major source of the silylsilylene radical, Si_2H_4B, which is highly reactive and plays an important role in cluster growth, and furthermore the branching ratio is rather sensitive to pressure. Around atmospheric pressure, in contrast, these reactions tend to produce disilane, which is relatively stable, and the branching ratio is insensitive to pressure. Hence the effect of total pressure on particle nucleation in the two regimes is found to be quite different.

Finally, Fig. 11 shows the effect of varying the silane flow rate. Convection transports particles toward the heated substrate, while thermophoresis pushes particles away. For sufficiently low flow rates thermophoresis dominates, producing larger particle concentrations near the inlet than near the substrate. These particles have a relatively long residence time, and thus grow to larger sizes.

Summary

A detailed model has been developed to describe particle nucleation during thermal decomposition of silane. This model includes detailed pyrolysis and clustering kinetics for a large number of silicon hydrides containing up to ten silicon atoms. The chemical clustering model has been coupled to an aerosol dynamics moment model. Zero-dimensional and stagnation-point flow simulations were conducted to examine the effects of carrier gas, temperature, pressure, silane concentration, and flow rate. The model predictions for the effects of these parameters are in good qualitative accord with previous experimental observations. A detailed comparison of the model predictions to recent experiments in an LPCVD system[38] will be presented in a subsequent publication.

Acknowledgments

This work was partially supported by Advanced Silicon Materials, Inc., the Semiconductor Research Corporation, the National Science Foundation (ECS-9731568 and CTS-9909563), and the University of Minnesota Supercomputing Institute.

References

1. A. Yuuki, Y. Matsui, and K. Tachibana, *Jpn. J. Appl. Phys.*, **26**, 747 (1987).
2. C. J. Giunta, R. J. McCurdy, J. D. Chapple-Sokol, and R. G. Gordon, *J. Appl. Phys.*, **67**, 1062 (1990).
3. M. Frenklach, L. Ting, H. Wang, and M. J. Rabinowitz, *Israel J. Chem.*, **36**, 293 (1996).
4. M. T. Swihart and S. L. Girshick, *J. Phys. Chem. B*, **103**, 64 (1999).
5. P. Ho, M. E. Coltrin, and W. G. Breiland, *J. Phys. Chem.*, **98**, 10138 (1994).
6. R. G. Gilbert, K. Luther, and J. Troe, *Ber. Bunsenges. Phys. Chem.*, **87**, 169 (1983).
7. J. M. Jasinski, R. Becerra, and R. Walsh, *Chem. Rev.*, **95**, 1203 (1995).
8. J. G. Martin, H. E. O'Neal, and M. A. Ring, *Intl. J. Chem. Kinet.*, **22**, 613 (1990).
9. H. K. Moffat, K. F. Jensen, and R. W. Carr, *J. Phys. Chem.*, **95**, 145 (1991).
10. H. K. Moffat, K. F. Jensen, and R. W. Carr, *J. Phys. Chem.*, **96**, 7683 (1992).
11. H. K. Moffat, K. F. Jensen, and R. W. Carr, *J. Phys. Chem.*, **96**, 7695 (1992).
12. R. Becerra, H. M. Frey, B. P. Mason, R. Walsh, and M. S. Gordon, *J. Chem. Soc., Faraday Trans.*, **91**, 2723 (1995).

S0013-4651(00)02-051-6 CCC: $7.00

13. M. S. Gordon, T. N. Truong, and E. K. Bonderson, *J. Am. Chem. Soc*., **108**, 1421 (1986).
14. M. S. Gordon, D. R. Gano, J. S. Binkley, and M. J. Frisch, *J. Am. Chem. Soc*., **108**, 2191 (1986).
15. M. S. Gordon, J. S. Francisco, and H. B. Schlegel, *Adv. Silicon Chem*., **2**, 137 (1993).
16. M. T. Swihart and R. W. Carr, *J. Phys. Chem. A*, **101**, 7434 (1997).
17. S. W. Benson, *Thermochemical Kinetics: Methods for the Estimation of Thermochemical Data and Rate Parameters*, 2nd ed., Wiley, New York (1976).
18. M. T. Swihart and R. W. Carr, *J. Phys. Chem. A*, **102**, 785 (1998).
19. G. Katzer, M. C. Ernst, A. F. Sax, and J. Kalcher, *J. Phys. Chem. A*, **101**, 3942 (1997).
20. E. R. Ritter and J. W. Bozzelli, *Int. J. Chem. Kinet*., **23**, 767 (1991).
21. M. T. Swihart and S. L. Girshick, *Chem. Phys. Lett*., **307**, 527 (1999).
22. R. J. Kee, F. Rupley, E. Meeks, and J. A. Miller, Sandia National Laboratories Report no. SAND96-8216, Albuquerque, NM (1996).
23. N. Rao, S. Girshick, J. Heberlein, P. McMurry, M. Bench, S. Jones, D. Hansen, and B. Micheel, *Plasma Chem. Plasma Process*., **15**, 581 (1995).
24. S. K. Friedlander, *Ann. N. Y. Acad. Sci*., **404**, 354 (1983).
25. D. R. Warren and J. H. Seinfeld, *Aerosol Sci. Technol*., **3**, 135 (1984).
26. D. R. Warren and J. H. Seinfeld, *Aerosol Sci. Tech*., **4**, 31 (1985).
27. M. Frencklach and S. J. Harris, *J. Coll. Interface Sci*., **118**, 252 (1987).
28. S. E. Pratsinis and K.-S. Kim, *J. Aerosol Sci*., **20**, 101 (1989).
29. S. E. Pratsinis, *J. Coll. Interface Sci*., **124**, 416 (1988).
30. G. M. Phanse and S. E. Pratsinis, *Aerosol Sci. Technol*., **11**, 100 (1989).
31. S. K. Friedlander, *Smoke, Dust and Haze: Fundamentals of Aerosol Behavior*, Wiley, New York (1977).
32. A. E. Lutz, R. J. Kee, and J. A. Miller, Sandia National Laboratories Report SAND87-8248 Revised, Albuquerque, NM (1997).
33. M. E. Coltrin, R. J. Kee, G. H. Evans, E. Meeks, F. M. Rupley, and J. F. Grcar, Sandia National Laboratories Report SAND91-8005, Albuquerque, NM (1991).
34. F. Slootman and J.-C. Parent, *J. Aerosol Sci*., **25**, 15 (1994).
35. J. H. Seinfeld and S. N. Pandis, *Atmospheric Chemistry and Physics: From Air Pollution to Climate Change*, Wiley, New York (1998).
36. G. D. Ulrich, *Combustion Sci. Technol*., **4**, 47 (1971).
37. F. S. Lai, S. K. Friedlander, J. Pich, and G. M. Hidy, *J. Coll. Interface Sci*., **39**, 395 (1972).
38. S. Nijhawan, Ph.D. Dissertation, University of Minnesota, Minneapolis, MN (1999).
39. P. J. Ziemann, P. Liu, N. P. Rao, D. B. Kittelson, and P. H. McMurry, *J. Aerosol Sci*., **26**, 745 (1995).
40. S. Bhargava, M.S. Thesis, University of Minnesota, Minneapolis, MN (1999).